Langmuir

Article

pubs.acs.org/Langmuir

Chiral Distortion of Confined Ice Oligomers (n = 5,6)

Haifeng Ma,[†,§] Yun Ding,[‡] Marcella Iannuzzi,[‡] Thomas Brugger,[†] Simon Berner,[†] Jürg Hutter,[‡] Jürg Osterwalder,[†] and Thomas Greber*[,†]

[†]Physik-Institut and [‡]Physikalisch-Chemisches Institut, Universität Zürich, Winterthurerstrasse 190, CH-8057 Zürich, Switzerland

ABSTRACT: Ice nuclei have been studied on the hexagonal boron nitride nanomesh (h-BN/Rh(111)), a template with 2 nm wide molecule traps. Scanning tunneling microscopy shows confined clusters, where oligomers with three protrusions are particularly abundant. Together with local barrier height dI/dz maps, it is found that the dipoles of the water molecules arrange in a homodrome, which is consistent with density functional theory calculations. Hydrogen bonds toward the substrate identify h-BN/Rh(111) to be hydrophilic. The substrate distorts the hexamers (n = 6) and possibly pentamers (n = 5), where the experimentally observed footprints of the three protrusions appear more chiral than expected.

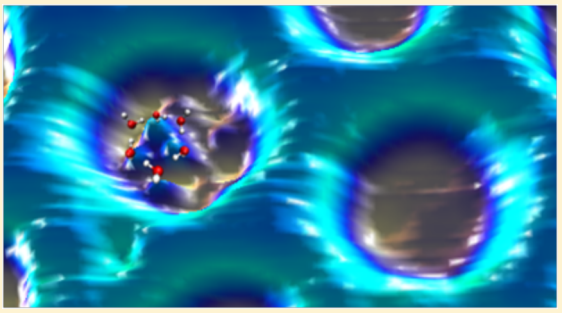

Confinement drives matter into aggregates with properties distinct from the unperturbed situation. It implies symmetry breaking and different reaction kinetics. This also holds for water, which is essential in many processes.[1] The confinement on surfaces depends on the wetting behavior, that is, on whether the substrate is hydrophobic or hydrophilic.[2−4] If water is further confined like, for example, in reverse micelles, the wetting layers bend and this causes again new properties.[5] Here nanoconfinement on the h-BN nanomesh template[6] is reported. h-BN/Rh(111) features a laboratory with nanometer sized "test-tubes" where hundreds of processes and its diversifications can be studied under the same conditions.[7] The template consists of a corrugated monolayer of hexagonal boron nitride on a rhodium (111) substrate, where the lattice mismatch and the relatively strong anisotropic bonding within the unit cell lead to a superstructure with 3.2 nm lattice constant and 2 nm "holes"[8,9] or "pores".[10] These pores act as molecular traps, where their rims house dipole rings, which constitute a lateral electrostatic trapping potential.[11]

The method of choice for the observation of single water molecules, their diffusion, and self-assembly is scanning tunneling microscopy.[12−14] In this Article, low coverages of water are investigated at 34 K. It turns out that ice oligomers with three visible molecules are particularly stable. Scanning tunneling microscopy (STM) images and local tunneling barrier height maps give a detailed view of the atomic structure, which is in accordance with density functional theory (DFT) for hexamers and possibly pentamers. The footprints of the observed oligomers display a higher chirality than expected from theory at 0 K.

Figure 1 shows the h-BN/Rh(111) template after exposure to 0.001 Langmuir of water on the surface at 34 K. Five single protrusions, two triple protrusion clusters in six different pores, and one single protrusion on the wires of the nanomesh are seen. All clusters display with a height similar to that of the wires (40 pm) and a diameter of 0.2 ± 0.05 nm. The distribution in the individual pores is not Poisson-like, which is a hint for diffusion and self-assembly. In this paper, we focus on the particularly abundant triple protrusion clusters inside the pores of h-BN nanomesh, which have an average size of 0.46 nm. Comparison with the water−water bond length in ice of ∼0.27 nm implies that these clusters stabilize more than three water molecules.

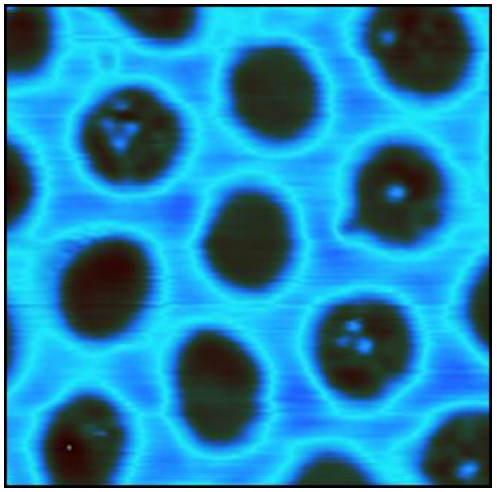

Figure 1. Ice clusters on h-BN nanomesh. STM image of the h-BN/Rh(111) nanomesh with small ice clusters at 34 K (10 × 10 nm^2). The clusters self-assemble inside the 2 nm pores. The predominant species are single- and triple-protrusion clusters. Here we focus on the triple protrusions. The image was acquired at V_s = −0.02 V and I_t = 50 pA.

Figure 2a shows one triple protrusion out of Figure 1. From the above geometric considerations, the ice rules, the hydrogen

Received: June 26, 2012
Revised: October 2, 2012
Published: October 5, 2012

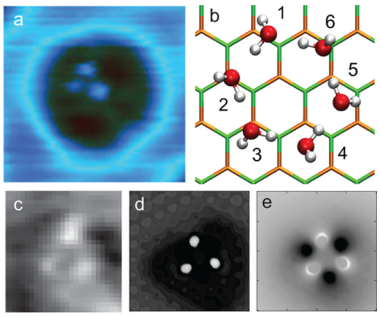

Figure 2. dI/dz spectroscopy map and structural model for the ice hexamer. (a) STM image of a single ice hexamer in a pore (3×3 nm^2, $V_s = -0.02$ V, and $I_t = 50$ pA). (b) Optimized geometric model on *h*-BN/Rh(111). It has a homodromic bilayer structure, where the three molecules in the top layer (even numbers) have dangling hydrogen atoms. The other three in the bottom layer display hydrogen bonding to the nitrogen atoms (green sticks) of the surface. (c) dI/dz spectroscopy map for the hexamer in (a). White color corresponds to a large local work function. (d) Simulated STM topography. (e) Simulated electrostatic potential image. For details, see the text.

bonds to the substrate,[15] and the measurement of the local tunneling barrier (see Figure 2c), we derive the structural model, which was confirmed by DFT calculations.[16] Reference 16 contains more theoretical results for a series of different water clusters on *h*-BN/Rh(111). On *h*-BN, ice pentamers also display with three protrusions (see below), though not as equilateral triangles. In Figure 2b, the DFT hexamer geometry is shown. The ice rules are satisfied: three hydrogen bonds to the substrate are found, and *every* water molecule provides a proton for a hydrogen bond to one of its neighbors. A configuration where every water molecule provides one proton for a hydrogen bond to one of its neighbors we call a homodrome.[13] This imposes for the water molecules labeled with *1*−*6* a sense of "rotation"; in Figure 2, they are arranged anticlockwise. "Sense of rotation" means that molecule *1* directs a proton to molecule *2* and molecule *2* to molecule *3*, and so forth. Of course, the clockwise homodrome is also possible and has the same energy. The odd water molecules *1*, *3*, and *5* lie closer to the substrate. Each one contributes one proton to the hydrogen bonds in the hexamer and one proton to the substrate. The even molecules *2*, *4*, and *6* are outermost and offer one proton each to the homodrome, and the remaining protons dangle into the vacuum. In the calculations, the O−O nearest neighbor distances turn out to be almost equal (0.273 ± 0.002 nm) and show no sizable "Kekulé-like" alternation as it was found for $(H_2O)_6$ on Cu(111), which is considered to be hydrophobic.[13]

The orientations of the water dipoles can be identified by local barrier height dI/dz spectroscopy maps that access the local work function, that is, the electrostatic potential.[15,17] Figure 2c shows the dI/dz map of the hexamer in Figure 2a. The protrusions correspond to high local work function patches. Therefore, the molecules that are responsible for the topographic contrast have a high local work function. The average distance between the patches appears 10% larger than the topographic protrusions. Therefore, the local work function maxima do not exactly coincide with the topographic protrusions; that is, the two images in Figure 2a and c contain complementary information. However, we do not see a significant "rotation" of the electrostatic triangle with respect to the topographic triangle and thus the sense of rotation of the homodrome. As mentioned above, the dipoles of the individual water molecules imply that the molecules with the hydrogens pointing to the substrate (odd numbers) have a high electrostatic potential and STM shows them to form the topographic contrast. This is surprising, since these molecules are dimmer (less bright) in ice clusters[15] and they are closer to the substrate than those of the even number molecules. Apparently, the local density of states at the Fermi level has a stronger influence on the topography than the larger tunneling barrier due to the higher local work function.

In order to confirm the assignment that we see the lower water molecules in the ice hexamers on *h*-BN/Rh(111), STM images were simulated within the Tersoff−Hamann (TH) approximation, where the local density of states at the Fermi level *and* the electrostatic potential (tunneling barrier) are considered. Simulations of other isomers that satisfy the ice rules and have three hydrogen bonds to the substrate give no indication for other hexamers than homodromes which would be stable and display with three protrusions. Figure 2d shows the constant tunneling current simulation, which confirms that the lower (odd) water molecules are imaged as protrusions for the homodrome. Furthermore, the corresponding electrostatic potential of the cluster (Figure 2e) is also in line with the experiment. The larger distance between the high work function patches with respect to those of the topographic protrusions is reproduced within the TH picture. The theoretical dilation is 14% as compared to 10 ± 5% from the experiment.

A closer inspection does however indicate deviations from the ideal hexamer as shown in Figure 2b. Significant distortions of the almost equilateral triangle geometry are observed in the STM images. This is not expected from the incommensurability of the hexamers with the *h*-BN substrate, since both have C_3 symmetry.

Figure 3a shows more triple protrusion clusters *I*−*XII*, which are sorted into three categories: TC, TR, and TA. First, TC series-clusters *I*, *II*, and *III* represent single species sitting near the *center* of the *h*-BN/Rh(111) pores, where STM resolves no other molecules inside it. Second, TR series-clusters *IV*−*VI* represent single species near the *rim* of the pores. The most abundant TA series-clusters *VII*−*XII* present with *additional* aggregates in the same pore. To quantify the footprints, fits of three 2D Gaussians are applied to the visible molecules of each hexamer in Figure 3a. In the same way, the precise positions and sizes of the pores are determined by a 2D Gaussian fit. The corresponding results are given in the lower right corners of Figure 3a, where the white dashed rings mark the positions of the rims.

In Figure 3b, the orientations of the clusters are presented. The histogram shows that they are rotated by 30° with respect to the BN lattice which confirms the model of Figure 2b, where the odd water molecules bind to the nitrogen atoms on a $\sqrt{3} \times \sqrt{3}\,R30°$ unit cell of *h*-BN. The rotation angle with respect to the substrate is the same as for ice clusters trapped in the pores.[15]

Figure 3c shows the histogram of the triangle sides for the investigated clusters, where the average distance between two protrusions of 0.46 ± 0.1 nm coincides with the *c*-plane lattice constant of 0.45 nm in hexagonal ice. The large standard deviation suggests that the experimentally observed triple protrusions may have different size and shape. In other words, triple protrusion ice clusters on *h*-BN/Rh(111) distort. For the further discussion we define the *distortion* δ_Δ to be

dx.doi.org/10.1021/la302561r | *Langmuir* 2012, 28, 15246−15250

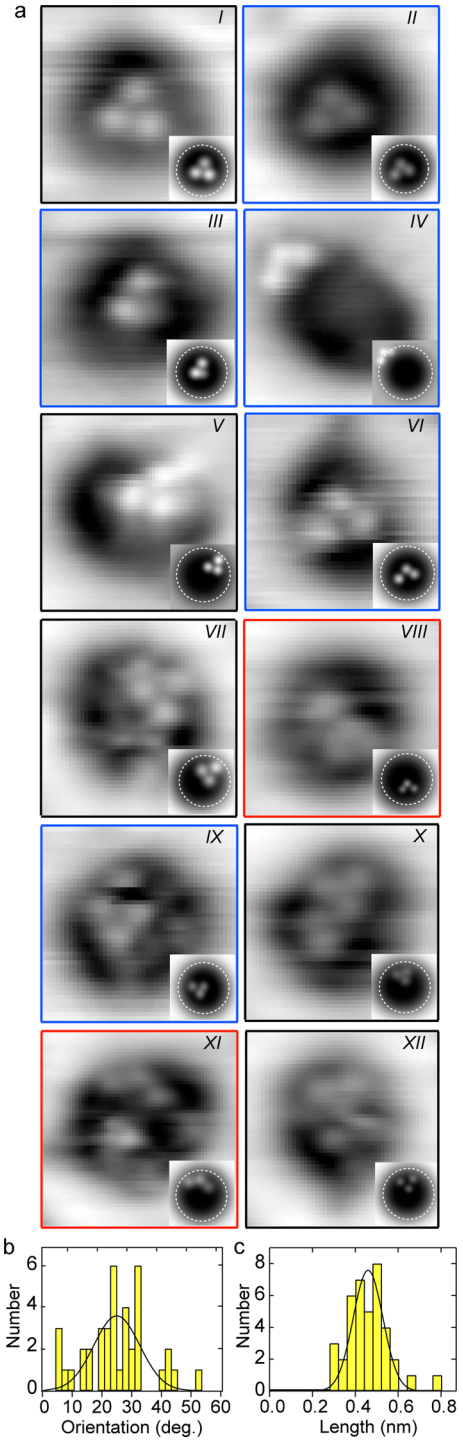

Figure 3. Distorted triple protrusion clusters. (a) STM images of species (*I*–*XII*) trapped in a pore (3 × 3 nm^2). The insets are 2D Gaussian fits for the pores and triple Gaussian fits for the triple protrusions. (b) Histogram of orientations with respect to the direction given by two neighboring pores. (c) Histogram of side lengths.

$$\delta_\Delta = \sqrt{(a-s)^2 + (b-s)^2 + (c-s)^2} \quad (1)$$

where a, b, c are the sides of the triangle and s is the average side length $(a + b + c)/3$. The experiments show an average $\bar{\delta}_\Delta$ of 0.24 ± 0.14s.

Inspection of the series indicates that most triple protrusions appear scalene, that is, are prochiral.[18] This calls for a chirality measure.[19] The geometric object "triangle" with sides a, b, c, where $a \neq b \neq c \neq a$, has a sense of rotation or chirality if seen from top (or from below).

We define a measure for *the chirality of a triangle bound to a surface* χ_Δ as[20]

$$\chi_\Delta = \frac{(a-b)(b-c)(c-a)}{(a+b+c)^3} \quad (2)$$

By convention, a, b, and c are arranged anticlockwise as seen from the top.

Figure 4 shows χ_Δ for the relative sides $\bar{a} = a/3s$ and $\bar{b} = b/3s$. The chirality χ_Δ between blue and red areas is zero as expected

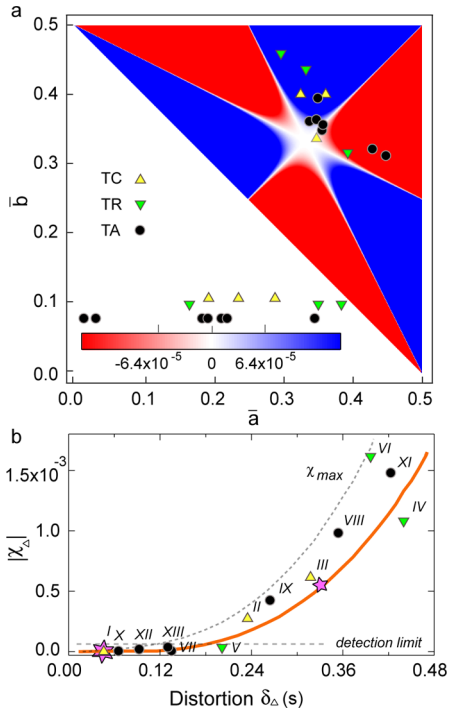

Figure 4. Chirality and distortion of triple protrusion ice clusters confined in the *h*-BN nanomesh. (a) Distribution of the chirality $\chi_\Delta(\bar{a},\bar{b})$ as defined in eq 2 for the clusters in Figures 3a and 2a. The axes show the relative triangle sides $(\bar{a}, \bar{b})$. The chiralities of TC, TR, and TA are expressed by the markers triangle-up, triangle-down, and circle, respectively. They are also lined up above the inset color scale bar, where the central tick indicates $\chi_\Delta = 0$, and the left and right ticks the detection limit $\chi_\Delta = \pm\ 6.4 \times 10^{-5}$. (b) Plot of the absolute chiralities $|\chi_\Delta|$ versus the distortion δ_Δ in units of average side length s. Above the detection limit, one out of seven hexamers has a chirality lower than the average $|\bar{\chi}_\Delta|$ from a random distribution (yellow line). The dotted line shows the maximum chirality for a given distortion. The values of the theoretical hexamer are marked with a purple six pointed star, and those for the pentamer with a five pointed star. For details, see the text.

for equilateral and isosceles triangles. For the hexamers shown in Figure 3a, c is set without loss of generality, to be the shortest side. Therefore, when $a > b$, χ_Δ is negative (red), and when $a < b$, χ_Δ is positive (blue). We find both chiralities, and neither is dominant, which is consistent with the fact the substrate has mirror symmetry.[21]

The $\delta_\Delta^{\mathrm{theo}}(H)$ of 0.044s and $\chi_\Delta^{\mathrm{theo}}(H)$ of 2.9 × 10^{-6} for the calculated ice hexamer in Figure 2d signal small distortion and chirality. The experimental $\delta_\Delta^{\mathrm{exp}}$'s and $|\chi_\Delta^{\mathrm{exp}}|$'s are larger. Further DFT simulations of ice heptamers do not explain this

dx.doi.org/10.1021/la302561r | *Langmuir* 2012, 28, 15246–15250

observation. However, some of the strongly distorted clusters (e.g., *III* and *VIII*) are close to the theoretical values $\delta_{\Delta}^{theo}(P)$ = 0.35 and $\chi_{\Delta}^{theo}(P)$ = 5.5 × 10^{-4} of the pentamer simulation shown in Figure 5. Although the water molecules in the

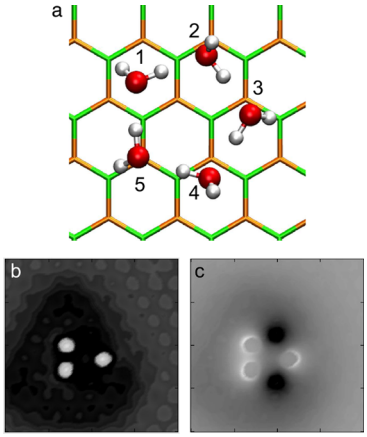

Figure 5. DFT structures for an ice pentamer on *h*-BN/Rh(111). (a) Optimized structure. Note in this example the homodromic arrangement of the water molecules is clockwise. The odd molecules 1, 3, and 5 like those for the hexamer in Figure 2 have a hydrogen bond to the substrate. (b) Simulated STM topography. (c) Simulated electrostatic potential image.

pentamer in Figure 5 have in average a 2.5 meV lower binding energy per water molecule than in the hexamer in Figure 2 where the bond energy is 430 meV per H_2O, their homodromic form is also stable in our DFT calculations. Furthermore, we want to emphasize that the transformation of a pentamer as shown in Figure 5 into a hexamer requires an additional water molecule and the breaking of a hydrogen bond in the homodrome of the pentamer. This possible observation of pentamers might also be important for the issue of pentagonal motivs of water chains on metal surfaces.[22] But also the calculated pentamer appears less chiral than the observed triple protrusion clusters with corresponding distortions. Of course, the experimental error in the determination of *a*, *b*, and *c* may produce an accidental distortion and chirality. In order to test whether the chirality is fortuitous, we plot in Figure 4b the average absolute chirality $|\overline{\chi}_{\Delta}|$ for a given distortion δ_{Δ} (yellow line). If chirality is not favored, we expect the experimental values to scatter around the yellow $|\overline{\chi}_{\Delta}|(\delta_{\Delta})$ line. It can, however, be seen that up to species *IV* all hexamers with $|\chi_{\Delta}|$ above the detection limit for chirality have a larger absolute chirality than expected from a random distortion. The detection limit is given by the accuracy of the determination of *a*,*b* and *c*, where a (conservative) limit of 10% relative error for the side length imposes $|\chi_{\Delta}| > 6.4 \times 10^{-5}$ to be significant.[20] *IV* is strongly distorted and belongs to the rim bound species, which suggests that the confining rim rather imposes equilateral than chiral distortions. The chirality is not induced by drift in the STM images since it is compensated perfectly by help of the known lattice of the (12 × 12) Rh(111) superstructure.[23] In addition, simulated double-tip STM images cannot explain the observations. Nevertheless, we do find chiral triple protrusion clusters inside the pores of the *h*-BN nanomesh, and the comparison with a random distortion indicates a nonstatistical distribution of the chirality. The implications of this finding may be reflected in the formation of amorphous ice,[24] or be important for the understanding of the formation of molecules on water solid interfaces. It will be interesting to investigate whether this expression is bound to confined water on a hydrophilic surface. In brackets, we note that a recent study on methanol hexamers on a gold surface also found chirality, which was associated to the hydrogen bond network in these structures.[25] For the understanding, we note that the distortions in the hydrogen bond network must impose significant anharmonicities in the interaction potentials. Furthermore, several competitive interactions contribute to the structure of the ice hexamers in the pores of *h*-BN nanomesh: the H−O bonds, the H−N bonds between the hexamer and the surface, as well as the electrostatic field induced α bonding due to the local work function gradient near the rims of the pores.[26] The subtle balance between the different interactions is proposed to lead to the formation of distorted structures and introduce the symmetry breaking, where left and right handed footprint structures occur with a higher preference than nonchiral ones.

In conclusion, nanoconfined ice hexamers on the *h*-BN/Rh(111) template are observed and identified. The observed distortions also suggest the possibility of stable pentamers. With scanning tunneling microscopy and local barrier height measurements, the arrangement of the molecules is inferred, where the corresponding homodromic model is consistent with density functional theory. The experiments indicate a significant distortion of the oligomer triple protrusion footprints with a particular peculiar affinity to a prochiral expression.

EXPERIMENTAL AND CALCULATIONAL DETAILS

Preparation and Characterization. The experiments were performed in an ultrahigh-vacuum (UHV) chamber with a background pressure below 4 × 10^{-10} mbar using a variable-temperature scanning tunneling microscope (Omicron VT-STM). The sample preparation included several cycles of Ar^+-bombardment, subsequent exposure to a few L (1 Langmuir = 10^{-6} Torr·s) of O_2, and annealing of the Rh(111) sample. Then it was exposed to 40 L of borazine $(HBNH)_3$ gas, while keeping the surface at 1070 K. This procedure yields a well-ordered large-scale single layer of hexagonal boron nitride on the Rh(111) surface. Milli-Q water was used and purified by several freeze-and-pump cycles. Water was introduced into the UHV chamber via a leak valve in the pressure range of 10^{-10}−10^{-8} Torr through a nozzle pointing toward the sample. All pressures and exposures correspond to the uncorrected reading of the ion gauge of the UHV chamber. In order to minimize tip induced H_2O motion on the surface, scanning parameters were set to the order of 50 pA for tunneling currents and −10 mV for tunneling voltages. STM images shown in this paper are obtained at 34 K.

Drift Corrections. All the STM images are corrected with a 2 × 2 matrix calibration:

$$M_{xy} = C \times M_{x^*y^*} \quad (3)$$

where matrix M_{xy} represents the (12 × 12)Rh supercell vectors of the *h*-BN nanomesh. Matrix $M_{x^*y^*}$ with two (12 × 12)Rh supercell vectors is obtained from the autocorrelation matrix of each STM image. From this the correction, matrix *C* is deduced.

Theoretical Calculations. All reported calculations were performed using the CP2K package[27] with the hybrid Gaussian and plane wave (GPW)[28] method. The revised PBE functional[29,30] and the Goedecker−Teter−Hutter(GTH)[31] pseudopotentials for all the DFT calculations were carried out concomitantly, and an additional empirical potential[32] was added for the dispersion correction. The substrate is a 13 × 13 boron nitride slab on top of four-layer 12 × 12 rhodium slabs and one Rh atom in the center of the pore.[8] Periodic boundary conditions are also applied.

The STM simulations are performed within the Tersoff−Hamann approximation. The height of the iso-current surface over the slab is

dx.doi.org/10.1021/la302561r | *Langmuir* 2012, 28, 15246−15250

determined at each (X,Y) position by the Z coordinate for which the quantity $n_b(Z)\exp[-2kR_0(\Phi(Z))^{1/2}]$ is constant. In the expression, n_b is the local density of states corresponding to the energy range $[E_{Fermi} + V_{bias}:E_{Fermi}]$, Φ is the local work function at the same position (X,Y,Z), R_0 is an estimate of the tip curvature radius, and $k = ((2m_e)^{1/2})/\hbar$. For the calculation of the reported images, the constant value is set at the center of the (X,Y) mesh, where the local density is equal to 8×10^{-6} electrons/Å^3. The bias potential V_{bias} is −0.5 eV, and the radius R_0 is equal to 2 Å. We also report the simulated local work function variations by mapping the electrostatic potential on the same iso-current surface obtained with the STM simulation.

AUTHOR INFORMATION

Corresponding Author

*E-mail: greber@physik.uzh.ch.

Present Address

[§]State Key Laboratory of Metastable Materials Science and Technology, Yanshan University, Qinhuangdao 066004, China.

Notes

The authors declare no competing financial interest.

ACKNOWLEDGMENTS

Financial support by the Swiss National Science Foundation is gratefully acknowledged. We acknowledge resources provided by the Swiss National Supercomputing Center CSCS.

REFERENCES

(1) *Water and Life:The Unique Properties of H_2O*; Lynden-Bell, R. M., Morris, S. C., Barrow, J. D., Finney, J. L., Harper, C., Eds.; CRC Press: Boca Raton, FL, 2010; p 396.

(2) Thiel, P. A.; Madey, T. E. The interaction of water with solid surfaces: Fundamental aspects. *Surf. Sci. Rep.* **1987**, *7*, 211−385.

(3) Henderson, M. A. The interaction of water with solid surfaces: fundamental aspects revisited. *Surf. Sci. Rep.* **2002**, *46*, 5−308.

(4) Hodgson, A.; Haq, S. Water adsorption and the wetting of metal surfaces. *Surf. Sci. Rep.* **2009**, *64*, 381−451.

(5) Hauser, H.; Haering, G.; Pande, A.; Luisi, P. L. Interaction of water with sodium bis(2-ethyl-1-hexyl) sulfosuccinate in reversed micelles. *J. Phys. Chem.* **1989**, *93*, 7869−7876.

(6) Corso, M.; Auwärter, W.; Muntwiler, M.; Tamai, A.; Greber, T.; Osterwalder, J. Boron Nitride Nanomesh. *Science* **2004**, *303*, 217−220.

(7) Ma, H.; Thomann, M.; Schmidlin, J.; Roth, S.; Morscher, M.; Greber, T. Corrugated single layer templates for molecules: From h-BN Nanomesh to Graphene based Quantum dot arrays. *Front. Phys. China* **2010**, *5*, 387−392.

(8) Laskowski, R.; Blaha, P.; Gallauner, T.; Schwarz, K. Single-Layer Model of the Hexagonal Boron Nitride Nanomesh on the Rh(111) Surface. *Phys. Rev. Lett.* **2007**, *98*, 106802−106806.

(9) Goriachko, A.; He, Y.; Knapp, M.; Over, H.; Corso, M.; Brugger, T.; Berner, S.; Osterwalder, J.; Greber, T. Self-Assembly of a Hexagonal Boron Nitride Nanomesh on Ru(0001). *Langmuir* **2007**, *23*, 2928−2931.

(10) Berner, S.; Corso, M.; Widmer, R.; Gröning, O.; Laskowski, R.; Blaha, P.; Schwarz, K.; Goriachko, A.; Over, H.; Gsell, S.; Schreck, M.; Sachdev, H.; Greber, T.; Osterwalder, J. Boron Nitride Nanomesh: Functionality from a Corrugated Monolayer. *Angew. Chem., Int. Ed.* **2007**, *46*, 5115−5119.

(11) Dil, H.; Lobo-Checa, J.; Laskowski, R.; Blaha, P.; Berner, S.; Osterwalder, J. Greber, Surface Trapping of Atoms and Molecules with Dipole Rings. *Science* **2008**, *319*, 1826−1829.

(12) Mitsui, T.; Rose, M. K.; Fomin, E.; Ogletree, D. F.; Salmeron, M. Water Diffusion and Clustering on Pd(111). *Science* **2002**, *297*, 1850−1852.

(13) Michaelides, A.; Morgenstern, K. Ice nanoclusters at hydrophobic metal surfaces. *Nat. Mater.* **2007**, *6*, 597−601.

(14) Kumagai, T.; Kaizu, M.; Okuyama, H.; Hatta, S.; Aruga, T.; Hamada, I.; Morikawa, Y. Water Monomer and Dimer on Cu(110) Studied Using a Scanning Tunneling Microscope. *e-J. Surf. Sci. Nanotechnol.* **2008**, *6*, 296−300.

(15) Ma, H.; Brugger, T.; Berner, S.; Iannuzzi, M.; Hutter, J.; Osterwalder, J.; Greber, T. Nano-ice on Boron Nitride Nanomesh: Accessing Proton Disorder. *ChemPhysChem* **2009**, *11*, 399−403.

(16) Ding, Y.; Iannuzzi, M.; Hutter, J. Investigation of Boron Nitride Nanomesh Interacting with Water. *J. Phys. Chem. C* **2011**, *115*, 13685−13692.

(17) Vitali, L.; Levita, G.; Ohmann, R.; Comisso, A.; Vita, A. D.; Kern, K. Portrait of the potential barrier at metal-organic nano-contacts. *Nat. Mater.* **2010**, *9*, 320−323.

(18) Eliel, E. L. Prostereoisomerism (prochirality). In *Topics in Current Chemistry*; Springer-Verlag: Heidelberg, 1982; Vol. *105*, pp 1−76.

(19) Petitjean, M. Chirality and Symmetry Measures: A Transdisciplinary Review. *Entropy* **2003**, *5*, 271−312.

(20) Ma, H.; Greber, T. A measure for the chirality of triangles. **2010**, arXiv:1011.0020v1. **2010**, arXiv.org e-Print archive. http://arxiv.org/abs/1011.0020; pp 387−392.

(21) Barlow, S. M.; Raval, R. Complex organic molecules at metal surfaces: bonding, organisation and chirality. *Surf. Sci. Rep.* **2003**, *50*, 201−341.

(22) Carrasco, J.; Michaelides, A.; Forster, M.; Haq, S.; Raval, R.; Hodgson, A. A one-dimensional ice structure built from pentagons. *Nat. Mater.* **2009**, *8*, 427−431.

(23) Bunk, O.; Corso, M.; Martoccia, D.; Herger, R.; Willmott, P.; Patterson, B.; Osterwalder, J.; van der Veen, J.; Greber, T. Surface X-ray diffraction study of boron-nitride nanomesh in air. *Surf. Sci.* **2007**, *601*, 7−10.

(24) Stevenson, K. P.; Kimmel, G. A.; Dohnáek, Z.; Smith, R. S.; Kay, B. D. Controlling the Morphology of Amorphous Solid Water. *Science* **1999**, *283*, 1505−1507.

(25) Lawton, T. J.; Carrasco, J.; Baber, A. E.; Michaelides, A.; Sykes, E. C. H. Visualization of Hydrogen Bonding and Associated Chirality in Methanol Hexamers. *Phys. Rev. Lett.* **2011**, *107*, 256101.

(26) Greber, T. Graphene and Hexagonal Boron Nitride Layers: Nanostructures with 3 bond hierarchy levels. *e-J. Surf. Sci. Nanotechnol.* **2010**, *8*, 62−64.

(27) CP2K is freely available from www.cp2k.org, 2009.

(28) Lippert, G.; Hutter, J.; Parrinello, M. A hybrid Gaussian and plane wave density functional scheme. *Mol. Phys.* **1997**, *92*, 477−487.

(29) Perdew, J.; Burke, K.; Ernzerhof, M. Generalized Gradient Approximation Made Simple. *Phys. Rev. Lett.* **1996**, *77*, 3865−3868.

(30) Zhang, Y.; Yang, W. Comment on "Generalized Gradient Approximation Made Simple". *Phys. Rev. Lett.* **1998**, *80*, 890−893.

(31) Goedecker, S.; Teter, M.; Hutter, J. Separable dual-space Gaussian pseudopotentials. *Phys. Rev. B* **1996**, *54*, 1703−1710.

(32) Grimme, S. Semiempirical GGA-type density functional constructed with a long-range dispersion correction. *J. Comput. Chem.* **2006**, *27*, 1787−1799.